NANO LETTERS

Letter

pubs.acs.org/NanoLett

Enhanced Optical Trapping and Arrangement of Nano-Objects in a Plasmonic Nanocavity

Chang Chen,[†,‡,¶] Mathieu L. Juan,[§,¶] Yi Li,[†,∥] Guido Maes,[‡] Gustaaf Borghs,[†,⊥] Pol Van Dorpe,*[,†,∥] and Romain Quidant*[,§,#]

[†]IMEC, kapeldreef 75, 3001 Leuven, Belgium

[‡]Department of Chemistry, Katholieke Universiteit Leuven, Celestijnenlaan 200F, 3001 Leuven, Belgium

[§]ICFO-Institut de Ciences Fotoniques, Mediterranean Technology Park, 08860 Castelldefels, Spain

[∥]Department of Electrical Engineering, Katholieke Universiteit Leuven, Kasteelpark Arenberg 10, 3001 Leuven, Belgium

[⊥]Department of Physics and Astronomy, Katholieke Universiteit Leuven, Celestijnenlaan 200D, 3001 Leuven, Belgium

[#]ICREA-Institució Catalana de Recerca i Estudis Avançats, Barcelona, 08010, Spain

Supporting Information

ABSTRACT: Gentle manipulation of micrometer-sized dielectric objects with optical forces has found many applications in both life and physical sciences. To further extend optical trapping toward the true nanometer scale, we present an original approach combining self-induced back action (SIBA) trapping with the latest advances in nanoscale plasmon engineering. The designed resonant trap, formed by a rectangular plasmonic nanopore, is successfully tested on 22 nm polystyrene beads, showing both single- and double-bead trapping events. The mechanism responsible for the higher stability of the double-bead trapping is discussed, in light of the statistical analysis of the experimental data and numerical calculations. Furthermore, we propose a figure of merit that we use to quantify the achieved trapping efficiency and compare it to prior optical nanotweezers. Our approach may open new routes toward ultra-accurate immobilization and arrangement of nanoscale objects, such as biomolecules.

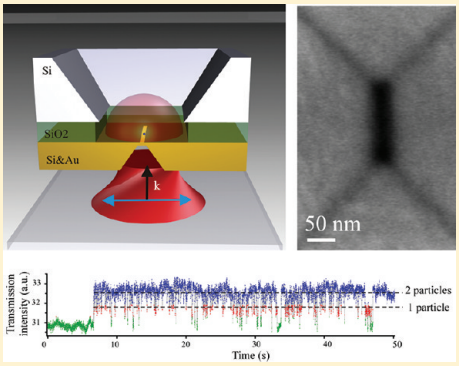

KEYWORDS: *Plasmonics, optical trapping, nanopore, arrangement*

The ability of surface plasmons (SPs) to concentrate light down to the nanometer scale already benefits to a broad range of applications including biochemical sensing,[1,2] biomedicine,[3,4] lithography,[5,6] high-resolution imaging,[7,8] solar cells,[9,10] and photonic devices.[11−13] Large plasmonic field gradients also offer strong optical force fields on a nearby object.[14] In the 1990s, SP-based trapping near metallic nanostructures has been predicted theoretically,[15,16] and more recently, experimentally demonstrated.[17−21]

Beyond permitting subwavelength trap sizes,[17,22,23] the recently proposed self-induced back action (SIBA) approach offers the unique advantage to achieve trapping with average local light intensities that are substantially smaller than prior approaches exclusively based on gradient forces.[20] Moderate local intensities are particularly critical to the trapping of nanoscaled objects that exhibit a similar refractive index but greater than the surrounding medium, such as nanometer dielectric particles, proteins, or viruses.[22] Indeed, for such small polarizabilities the high intensities required by conventional trapping are responsible for fast damage of the specimen due to heating.[24] By involving the active role of the trapped specimen in the trapping mechanism, the SIBA effect enables to dramatically relax the local intensity requirements.[20] The SIBA effect relies on the high sensitivity of the plasmonic structure to the position of the specimen. By properly engineering the plasmonic mode such that the local intensity within the trap is maximized when the specimen is trapped, the momentum of the (plasmonic) photons interacting with the specimen decreases as it moves out of the trap. Owing to momentum conservation, these changes create an additional restoring force field that is by definition automatically synchronized with the specimen's dynamics. Such dynamical reconfiguration of the trap enables overcoming the high-energy kicks experienced by the trapped object and consequently the use of significantly lower local field intensities. Yet, extending optical trapping to the nanometer regime with plasmonic tweezers raises the additional challenge of observing the trapped specimen. When its size reduces to tens of nanometers, only fluorescence measurements, when this applies,[19] and advanced scattering schemes[25−27] may enable monitoring the trapping events. Another advantage of an approach based on SIBA trapping is that one can exploit the existing sensitivity of the trapping plasmonic structure to the position of the

Received: September 9, 2011
Revised: November 23, 2011
Published: December 2, 2011

Downloaded via UNIVERSITE DE SHERBROOKE on August 11, 2025 at 18:48:50 (UTC).
See https://pubs.acs.org/sharingguidelines for options on how to legitimately share published articles.

 © 2011 American Chemical Society dx.doi.org/10.1021/nl2031458 | *Nano Lett.* 2012, 12, 125−132

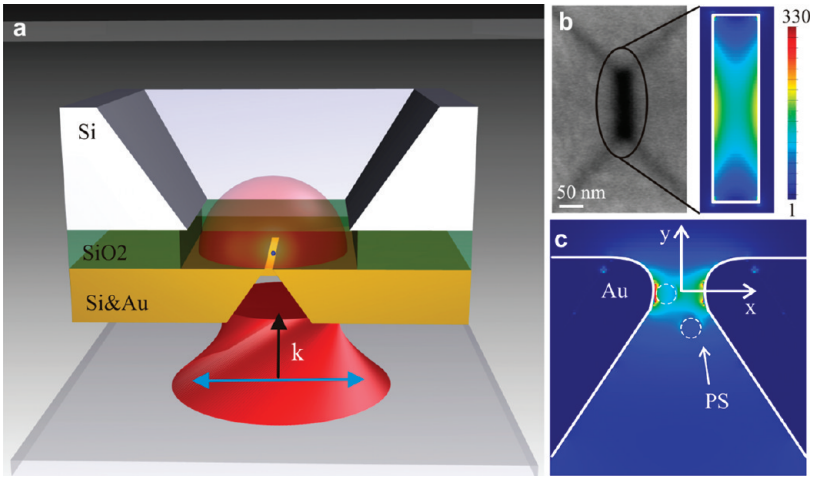

Figure 1. SIBA plasmonic trapping using a Fabry–Pérot nanopore cavity. (a) Schematic drawing of the trapping setup for a Fabry–Pérot nanopore (40 × 170 nm) in a freestanding silicon membrane coated with a 100 nm Au layer. The incident light is focused at the cavity, and the transmitted light is detected at the other side of the chip. A single PS bead (blue) is trapped inside the nanopore. (b) SEM image of the nanopore and FDTD simulated field distribution inside the pore at its resonance (top view). (c) FDTD simulated field distribution for the double-bead trapping (side view): The first PS bead is trapped by the hot spot at one of the nanopore edges, while the second one is approaching. The origin of the coordinate system is at the center of the nanopore where the gap size is the smallest.

specimen to sense the specimen presence through a change of the plasmon resonance. The first experimental implementation of SIBA trapping in a circular metallic aperture[20] demonstrated trapping of polystyrene (PS) beads down to 50 nm with local intensities as low as 10^9 W/m.

In order to achieve trapping of smaller low refractive index specimens, further design of the plasmonic aperture is required to maximize the SIBA effect. Here, we report on SIBA trapping of 22 nm PS beads in a rectangular plasmonic nanopore. Such a nanopore supports propagating gap plasmons that can be tuned by adjusting its geometrical aspect ratio. The supported Fabry–Pérot resonance is characterized by a highly confined field at the geometrical center, near the nanopore edges.[28] Moreover, it supplies a much stronger resonant transmission than a circular aperture of the same area. Single 22 nm PS beads were successfully trapped by using a near-infrared laser line. Double-bead trapping was also observed and appears to be the most probable event. The specificities of single- and two-bead trapping (lifetime, probability) along with the involved physical mechanism are discussed in view of statistical analysis of the trapping data and numerical simulations. Finally, a universal figure of merit (FoM) that aims at comparing the trapping efficiency of any trapping experiment, independently of the material of the trapped specimen and the trap configuration, is proposed and used to compare the different approaches.

The SIBA approach exploits the change in the plasmon resonance of the trapping structure induced by the presence of the specimen. For this perturbation to have a positive impact on the trapping efficiency, the presence of the object in the trap has to increase either the local field enhancement and/or its gradient.[20] In the case of an aperture in a metallic film, the effective local refractive index is increased as the object enters the close vicinity of the aperture inducing a red shift of SP resonance and consequently a change of the transmission and the local field enhancement at the trapping wavelength.

The SIBA effect can thus be achieved by designing the aperture such that it is slightly blue detuned in absence of any object. The red shift induced by the presence of the trapped object sets then the structure on resonance, increasing the optical near field. The far-field transmission is increased as well, providing a direct observable of the trapping dynamics that allows for the accurate and fast monitoring of the trapping events over time.

Similarly to what was done to improve the sensitivity of particle-based biomolecules sensors,[29] the impact of the trapped object can be further increased by properly engineering the aperture mode in order to achieve trapping of smaller particles. Further increasing the induced red shift of the resonance requires optimizing the spatial overlap between the mode volume and the specimen. While simply downscaling the diameter of a circular nanoaperture would lead to a fast decay of both the local field enhancement and the transmission intensity along with a blue shift of the resonance to spectral regions where absorption increases, another strategy is required.[20] Recently, Pang and collaborators demonstrated near-infrared trapping of 12 nm silica beads in double nanoholes.[30] Here, we chose to use a rectangular aperture (see Figure 1) that combines, upon an incident polarization along the short axis, the strongly confined SP gap mode (along the short axis) with a $\lambda_{SPP}/2$ Fabry–Pérot resonance along the long axis, leading to two regions with large field enhancement at the center of the nanopore, near the edges. The SP gap plasmon resonance not only generates a strong field intensity gradient facilitating trapping but also enhances the far-field light transmission,[28] enabling monitoring the trapping events despite the small aperture area. In order to obtain a slightly blue detuned resonance from the trapping wavelength, we designed a 40 × 170 nm^2 nanopore (as shown in Figure 1b). Such aperture supports a theoretical resonance centered at around 950 nm. In addition, due to the symmetry of the near-field distribution, for small enough particles (equal or smaller than 20 nm) this nanopore potentially enables simultaneous stable trapping of two particles, as shown in Figure 1c. Such trapping event yields interesting physics, as the first bead trapping will induce a subsequent field distribution inside the nanopore resulting in a different optical potential landscape for the second bead.

dx.doi.org/10.1021/nl2031458 | *Nano Lett.* 2012, 12, 125–132

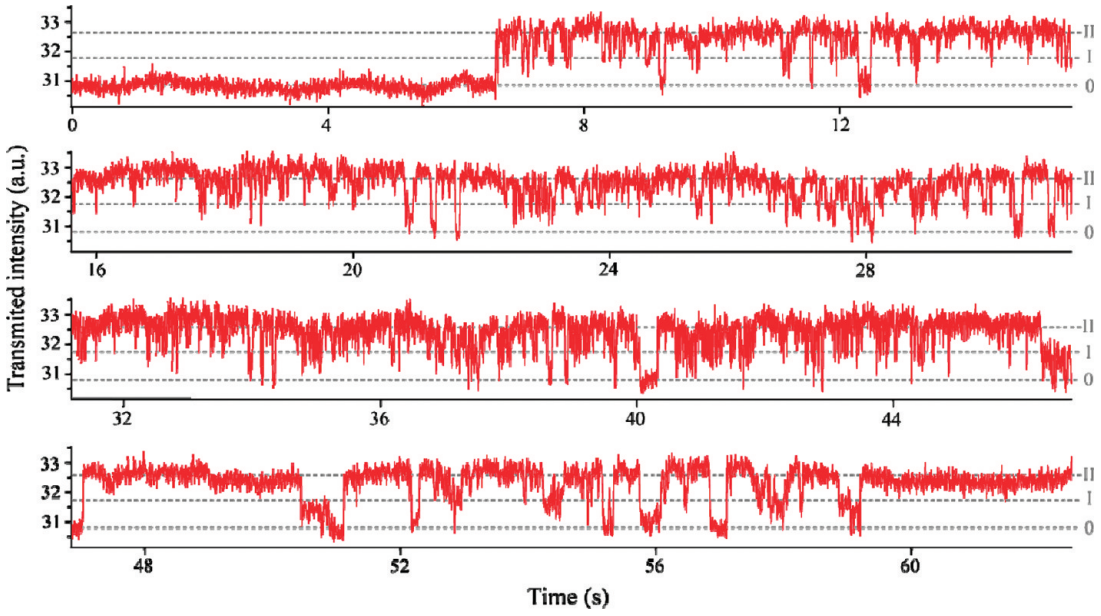

Figure 2. Selected plasmonic trapping sequences recorded over ~1 min. The dashed lines 0, I, and II represent the average transmission intensity when no beads, one bead, and two beads are trapped, respectively.

The gold rectangular nanopore was fabricated by micromachining the bottom of a prism-like cavity in a freestanding silicon membrane (see Methods Section). In the trapping experiment, the nanopore was sandwiched between two liquid chambers and the polystyrene beads (22 ± 4 nm) introduced exclusively in the bottom chamber. The incident 1064 nm Nd:YAG laser (2.5 mW) was slightly focused on the nanopore with its polarization perpendicular to the long axis of the aperture. The transmission signals were recorded on the other side of the membrane by using a silicon photodiode. More details about the experimental conditions can be found in the Methods Section.

Figure 2 displays an experimental 1 min time trace of the intensity transmitted through the nanopore. A statistical study of the distribution of transmission values reveals three main levels (see below and Figure 3) that appear as dashed lines in Figure 2. The constant increments between consecutive levels enable us to attribute these three levels to: (0) nontrapping, (I) single-bead trapping, and (II) double-bead trapping, respectively.

To get further insight into the statistics of the different trapping events, we first used an expectation maximization (EM) algorithm to analyze the 12 500 data points of Figure 2. The EM algorithm is a parameter-free iterative method for finding the maximum likelihood of a histogram.[31] The histogram obtained using this technique is shown in Figure 3a, underlining the three different trapping states. Supposing all states have Gaussian distributions, we can fit the data obtained with the EM method using a Gaussian mixture model. The first Gaussian distribution (state 0, green curve) corresponds to the nontrapping event. The transmission has a mean intensity of 30.8, and its weight is 13.1%. It should be noticed that this weight, the integrated probability under the Gaussian fit, is associated to the considered finite sequence. In a long-time measurement, the nontrapping situation would be dominant, leading to a much narrower and stronger Gaussian peak. The second Gaussian distribution (state I, red curve) corresponds to the single-bead trapping events, with a mean intensity of 31.8 and a weight of 22%, while the third Gaussian distribution (state II, blue curve) corresponds to the double-bead trapping events, with a mean intensity of 32.7 and the weight of 64.8%. The average intensity values obtained with this statistical analysis provide reference values (dashed lines of the Figure 2) to differentiate the three trapping states 0, I, and II. In addition, the weight of each Gaussian fit gives the total state occupancy, clearly showing higher probability of double-bead trapping. Since the transmission intensity fluctuations for a given trapping state are directly related to the spatial distribution of the trapped object, the line width of the Gaussian fits is directly related to the trapped object confinement. From the numerical calculations the confinement is expected to be of few nanometers along the x-direction for the single-bead trapping. Indeed, for a bead traveling away from the edge, the transmission fluctuations are around 5% (see Supporting Information), in fair agreement with the 3.5% observed in the experiment.

In order to retrieve the transition rate between the different states, we also applied an algorithm based on the hidden Markov model (HMM) to calculate the transition rate and state lifetime from the time trace.[32] The different transmission intensity values can be directly related to the trapping state in the nanopore. By treating the complete time trace presented in Figure 2, we obtained the Markov diagram of Figure 3b. From this data, we observe a very low transition rate between the states 0 and II, meaning that within the sampling rate time scale, when two beads are trapped, they enter the trap successively. In addition, state II shows a higher stability than state I with 97.18% and 71.26%, respectively. In terms of release rate (inverse of trapping time), state I has a 10 times larger release rate than that of state II. While the reached trapping time for single bead event is very short (0.1 s), it has to be compared to the diffusion constant of 25 $\mu m^2 \cdot s^{-1}$ for a single 22 nm polystyrene bead in water at 300 K (67 μs to cover 100 nm). Double-bead trapping shows substantially longer trapping times, reaching 3.5 s. This statistical study underlines the

dx.doi.org/10.1021/nl2031458 | Nano Lett. 2012, 12, 125−132

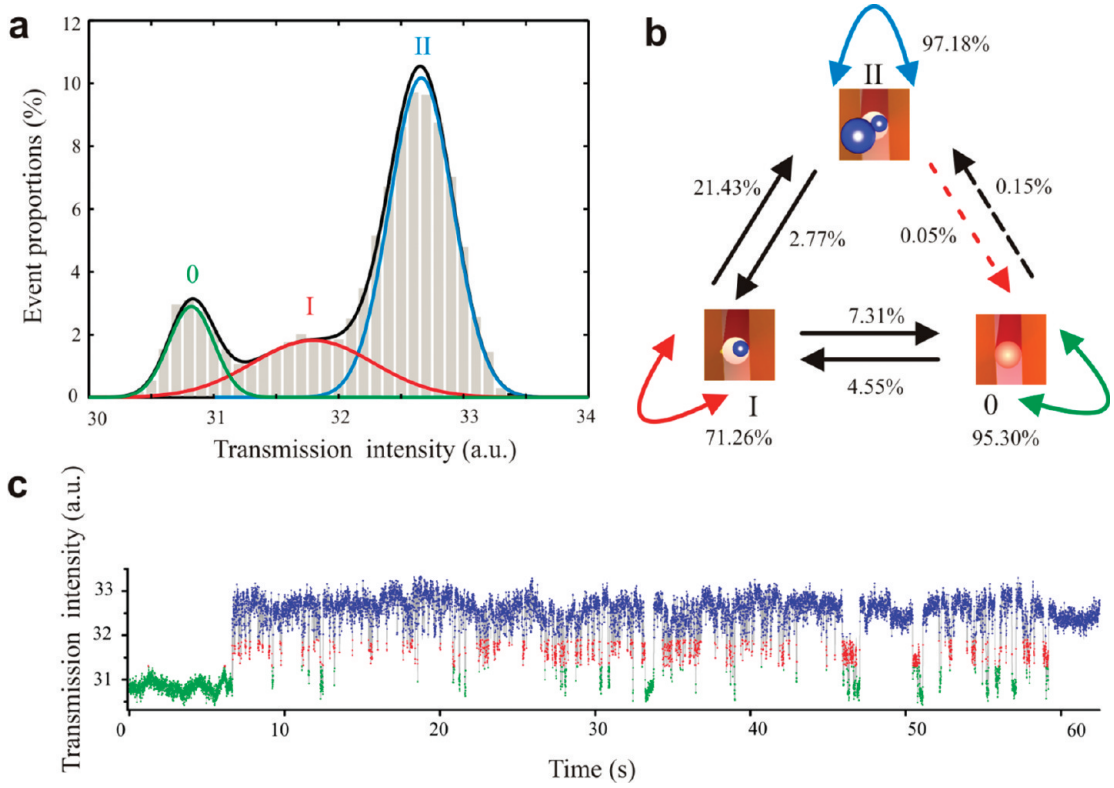

Figure 3. Statistic analysis of trapping. (a) Transmission intensity histogram of trapping events shown in Figure 3, including Gaussian fits based on EM algorithm. The three peaks correspond to: nontrapping state (0), single-bead trapping state (I), and double-bead trapping state (II). (b) Markov diagram of the state transition of the trapping events shown in Figure 2. (c) Discrimination of three states of trapping based on the HMM method.

cumulative aspect of the SIBA effect for a second bead entering the trap, as further discussed below.

In order to support our experimental data and get further insight into the trapping mechanism, we performed extensive numerical calculations obtained with commercial 3D finite difference time domain (FDTD) software (see Methods Section). Based on the intended geometrical parameters of the fabricated nanopore, we first computed the optical near field in the presence of the bead. For each position, the corresponding optical force was determined by calculating the Maxwell stress tensor (MST). Figure 4a displays the field intensity distribution obtained when a 20 nm PS bead is placed at the center of the nanopore, defined as the origin of the coordinate system. Due to the high degree of symmetry at this position, all forces cancel out producing an instable equilibrium. Indeed, a small position change would break the symmetry, and the bead would feel the force from the closest edge. As indicated in Figure 4b, the plasmonic field exerts a strong force on the bead along the x-direction (F_x), driving it predominantly toward the edge. Moreover, while approaching the edge, the force magnitude increases monotonously. Along the y-direction (direction of light propagation), the force F_y changes its sign across the nanopore (Figure 4c), showing the attractive force toward the pore. This attractive force toward the center of cavity also exists along the z-direction (Figure 4c), caused by the Fabry–Pérot resonance. However, due to the larger spatial extension of the Fabry–Pérot mode, the force along the z-direction F_z varies slower, giving rise to a 1 order of magnitude lower stiffness than for the x- and y-directions. Using the MST method, we calculated maximum values of the trapping stiffness for 1 W of injected power of 0.33, 0.16, and 0.018 pN/nm for the 20 nm bead along x-, y-, and z-directions, respectively. The forces along the y- and z- directions are attractive toward $y = 0$ and $z = 0$ plane, respectively, while the force along x pushes the object against the edge. The presence of two well-defined stable positions favors double-bead trapping.

While the mechanism for single-bead trapping is similar to the one observed in reference 20, double-bead trapping reveals some additional cumulative SIBA trapping enhancement effect that makes it the most probable trapping event. In the following, we simulated self-consistently (i.e., accounting for the presence of the bead(s) at each point) the force field for the single- and double-bead trapping (Figure 5a,b) by using the MST method. For the double-bead trapping, the second bead experiences the force field resulting from the presence of the first bead. Yet, due to the geometrical constraint in the nanopore, only few points can be calculated. Only considering remote positions for the double-bead event (e.g., $x = 8$ and $y = 20$ nm), the force experienced by the second bead is 9% stronger compared to single-bead trapping. In addition, it appears from the force field for single-bead trapping that the stable trapping position is slightly displaced toward the side of the nanopore. This small asymmetry arises from the asymmetrical shape of the aperture.

Further insight can be acquired by computing the transmission intensity through the nanopore and the field enhancement in the hot spots as functions of the wavelength. While the calculated transmission of an empty nanopore features a plasmon resonance centered at around 950 nm (Figure 6a), each consecutive trapping event (single and double) induces a resonance shift of about 5 nm that is responsible for a transmission change at the trapping wavelength. The transmission changes for one and two beads are 1.85 and 3.76% in the simulations and 3.16 and 5.97% in

dx.doi.org/10.1021/nl2031458 | Nano Lett. 2012, 12, 125–132

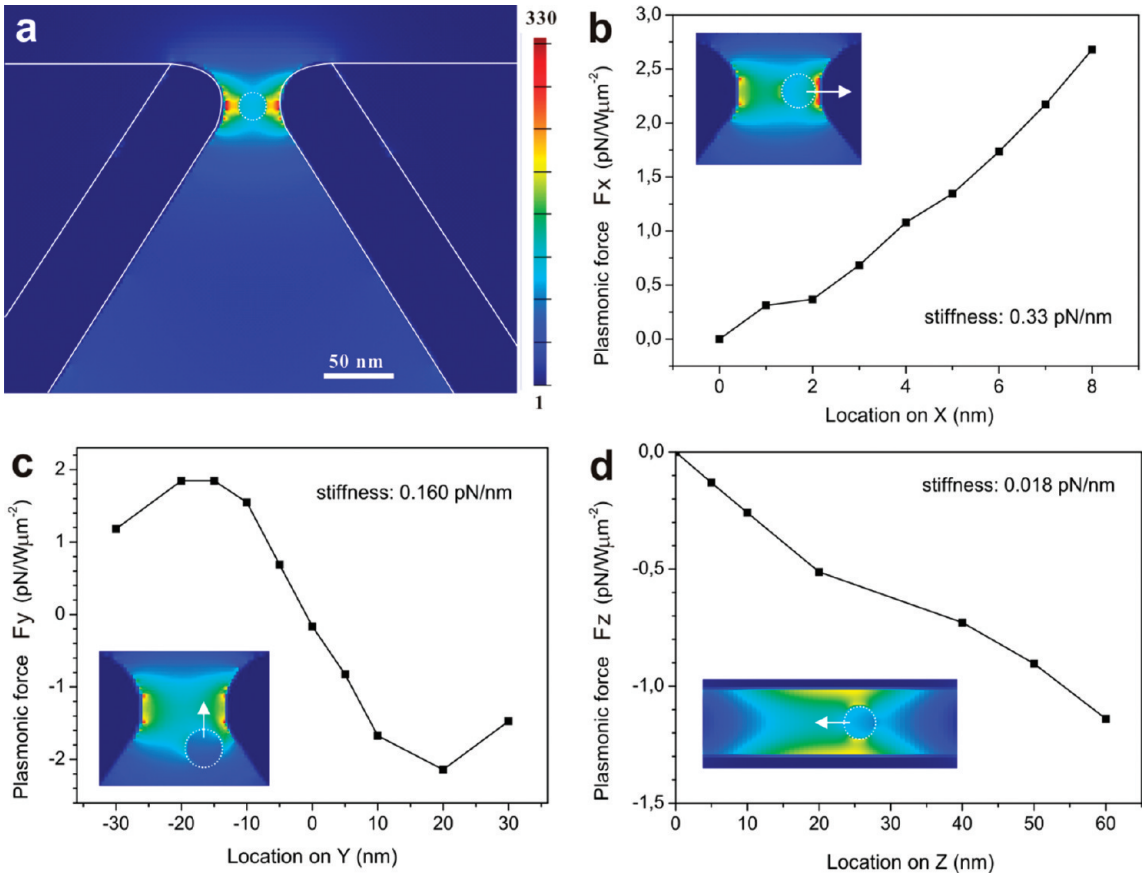

Figure 4. Numerical calculations on single bead trapping. (a) Optical field intensity profile (x, y) in the nanopore when one bead (with a radius of 10 nm) is located at the origin of the coordinate system. (b–d) Plasmonic trapping forces F_x, F_y, and F_z on the bead when it moves along the corresponding x-, y-, and z- axes, respectively.

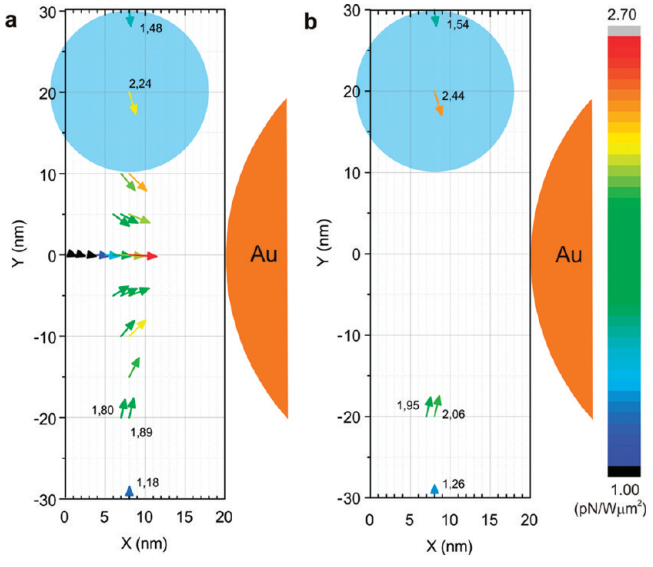

Figure 5. Numerical calculations of the single- and double-bead trapping. Force field maps inside the nanopore for (a) single- and (b) double-bead (with a radius of 10 nm) trapping obtained with the MST method. The forces are represented in both the color and the length (longer is stronger). The blue circle represents the PS bead, and the orange arc is the edge of the gold nanopore.

the experiment. In both simulated and experimental data, the transmission intensity change of the double-bead trapping is almost twice of that of the single-bead trapping. The higher values from the experiments are attributed to the morphological deviation between the simulated nanopore and the actual fabricated structure. Similar deviations were also observed for the circular nanopores.[20]

The enhancement spectra were taken at the lateral high-intensity regions at 1 nm away from the edge. As shown in Figure 6b, the main resonance bands appear at around 920 nm for both ground and trapping states. Despite the small influence of trapping on the spectral position of the resonance, a clear, stronger local field enhancement is observed. When located at the geometrical center of the nanopore, a single bead creates a slight increase of the local field enhancement as compared to the empty nanopore (solid red curve in Figure 6b). Conversely, this increase becomes substantially large when it sits near the edge (dashed red curve in Figure 6b). This illustrates the importance of the spatial overlap between the trapped beads and the electromagnetic modes of the nanopore.[33] For a double-bead trapping event, a much higher field enhancement factor is observed as each beads sits at the edges (Figure 6c), thus increasing the trapping potential depth and the lifetime of the double-bead trapping state. This underlines the possibility to optimize the plasmonic structure to trap a given number of objects and arrange them with a very high level of accuracy.

At this stage we are interested in comparing our approach with other nanotrapping approaches[17,19,20,23,25−27,34] and more generally provide a tool to compare different approaches. A direct comparison is though hindered by the differences in the

dx.doi.org/10.1021/nl2031458 | Nano Lett. 2012, 12, 125−132

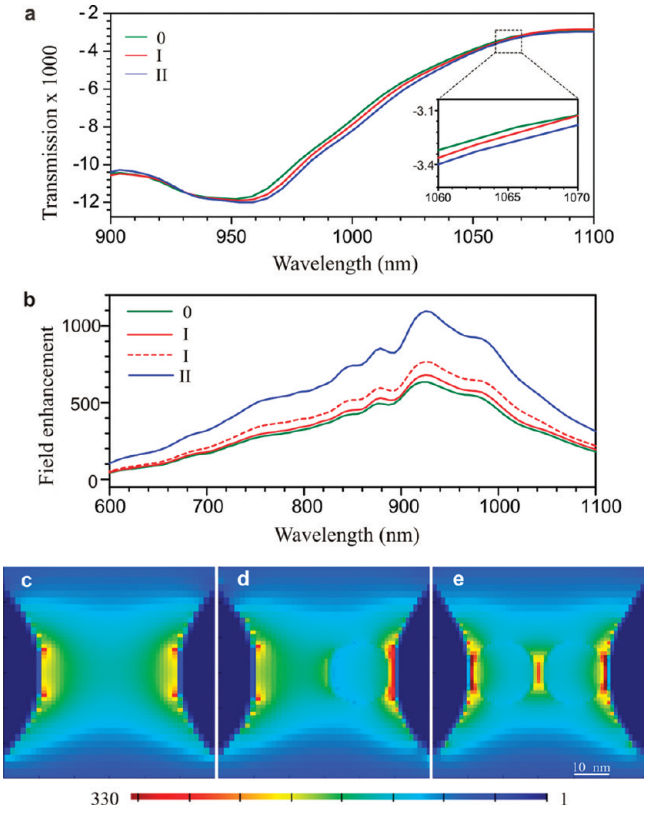

Figure 6. Variation of the optical properties during the trapping. The simulated the transmission spectra (a) and the field enhancement spectra (b) of non- (0), single- (I) and double- (II) bead (with a radius at 9 nm) in trapping. The solid and dash red curves correspond to the single-bead trapping at the center and the edge of the nanopore, respectively. (c–e) Field intensity distribution profiles (at 1064 nm) in the nanopore for the nonbead, single-, and double-bead trapping.

trapping configuration and the trapped specimen. To overcome this issue, we here introduce a FoM that aims at quantifying the trapping efficiency independently of the material of the trapped specimen and the incident and local field intensities.[35] Since the trapping force (gradient force in the Rayleigh regime using the point–dipole approximation)[36] is given by the polarizability and the field intensity gradient, we defined the FoM (in nm/W) as

$$\mathrm{FoM} = (I_{\mathrm{nor}} \times \alpha)^{-1} = (I_{\mathrm{inc}} \times \gamma \times \alpha)^{-1} \quad (1)$$

where I_{nor} is the normalized incident intensity given by the product of the incident intensity I_{inc} and the average value of the local intensity enhancement factor γ, and α is the polarizability (for more details see Supporting Information).

Conventional OT, formed at the tight focus of a laser beam, have allowed trapping of small (<50 nm) high refractive index particles (such as metallic or semiconductor nanocrystals) with high laser intensities[25−27,34] (>10^{12} W/m^2) featuring an absolute FoM from 10 up to 5 × 10^2 nm/W. Conversely, near-field-based approaches (either plasmonic or not) can dramatically increase the field gradient[17,19,34] to trap small (~200 nm) low refractive index dielectric objects. Remarkably, when applied to metallic nanoparticles, the SP-based approach can achieve trapping of 10 nm gold nanoparticles[23] with moderate intensities (10^{10}–10^{11} W/m^2) and a typical FoM of 2 × 10^3 nm/W.

Beyond, the SIBA strategy[20] provides an important improvement over previously achieved FoM. The original implementation of SIBA trapping in a circular metallic nanoapertures enabled trapping small dielectric objects, down to 50 nm, using a low incident intensity (~10^9 W/m^2) and a FoM of 9 × 10^3 nm/W (calculated from the 100 nm trapping). Such increase of the trapping ability can be graphically illustrated by plotting the different considered FoMs as a function of the specimen size (Figure 7). One can clearly observe that unlike the rest of

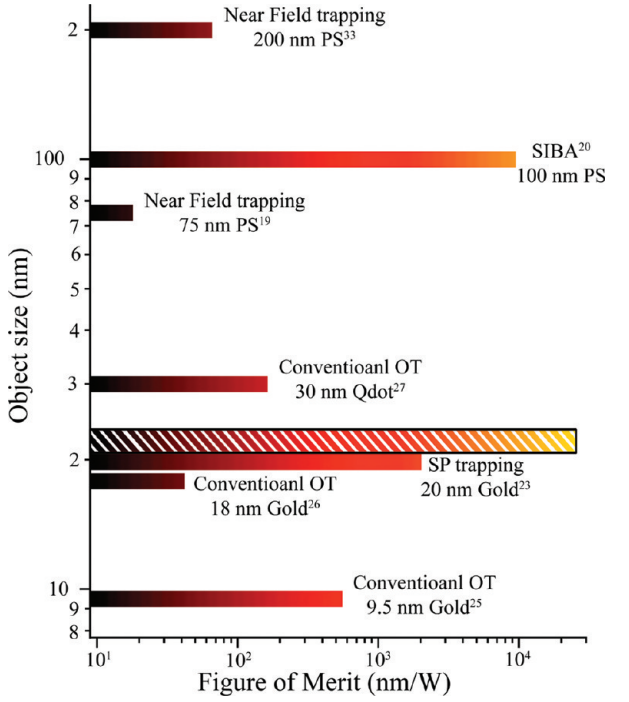

Figure 7. FoM for the different nanotrapping schemes. The graphic plots the FoM of trapping expriments discussed in refs 19, 20, 23, 25–27, and 34 as a function of the object size. The FoM of the current experiment is dashed.

approaches, SIBA trapping provides a higher FoM. With 1 × 10^4 nm/W, the FoM of the current experiment shows the highest FoM so far reported. Note that in addition to this necessary increase of the FoM to trap 22 nm PS beads, the improved sensing capability of the structure plays a crucial role for monitoring the different trapping events.

We demonstrated plasmonic trapping of nanoscaled dielectric (PS) beads with an average diameter of 22 ± 4 nm at low incident power. The trapping is achieved using the resonant excitation of gap plasmons in a Fabry–Pérot nanopore cavity. Relying on a SIBA strategy, the red shift induced by a bead in the nanopore increases the transmission intensity and trapping efficiency. While the feed-back effect of a single bead allows short trapping times, the effect is further enhanced if a second bead is trapped providing 1 order of magnitude longer trapping time for double-bead trapping. This cumulative aspect of the SIBA strategy enables new opportunities to trap a given number of objects. In addition, the arrangement of the trapped objects is directly related to the field distribution, in particular the localization of the intensity hot spots, allowing also the manipulation and alignment of elongated objects. The proposed approach opens the possibility to trap, sense, and arrange a given number of nanoscaled dielectric objects. In particular, the possible experimental

dx.doi.org/10.1021/nl2031458 | Nano Lett. 2012, 12, 125–132

realization of the sensing and control of DNA translocation through such nanopore.[37]

Methods. *Preparation of the Fabry–Pérot Nanopore Chips.* The nanopore chip was fabricated by standard nanofabrication procedures.[38] Briefly, electron beam lithography and silicon anisotropic wet etching (KOH etching) were used to form the nanopore on a freestanding Si membrane in a silicon-on-insulator chip. A similar process but based on UV lithography was used to form a large cavity on the backside silicon layer to generate an opened nanopore in the freestanding membrane. Consequently, a 100 nm gold layer is then deposited by a sputtering process. The resultant plasmonic nanopore is rectangular, with 40 nm in width and 170 nm in length. The depth of the top cavity was ~800 nm, while that of the back cavity was ~725 μm. The vertex of KOH etched silicon cavity was fixed at 70.5°. For characterization, the nanopore chips were observed using a scanning electron microscope (Philips, XL30 FESEM) at a 5 kV accelerated voltage.

Trapping Experiments. As shown in Figure 1, the oxygen plasma cleaned nanopore chip was placed on top of an aqueous chamber containing 0.05% w/v spherical PS beads with the size at 22 ± 4 nm (R25, Thermo Scientific) and 5% concentration of sodium dodecyl sulfate in the solution to inhibit agglomeration. The gold side of the chip was faced down to avoid gravity trapping. A second chamber only containing deionized water was placed on top of the chip to obtain uniform environments on both sides of the membrane. Cover glasses were used to form these temporary chambers. A continuous wave Nd:YAG laser with the wavelength of 1064 nm was focused onto the nanopore through a 40× microscope objective of 0.65 numerical aperture (Olympus PLN 40X). The focused spot is roughly at 2 μm in diameter. The incident power before the objective was 2.5 mW, leading to an intensity of 4.7×10^8 W/m^2 at the sample. The illumination was linearly polarized perpendicular to the longitudinal axis of the nanopore. The transmission intensity through the nanopore was recorded in real time with a 200 Hz sampling rate using a silicon photodiode placed on the other side of the chip. Additional details concerning the custom-built setup used were described in previous work.[20]

Numerical Simulations. 3D FDTD simulations were employed to solve Maxwell's equations for the complex Fabry–Pérot nanopore. Here, we used Lumerical FDTD Solutions v6.5 (Lumerical Solutions, Inc., Canada), which provides the distribution of both electromagnetic far and near fields supported by the structures. The detailed parameters set in the simulation were similar to our previous works,[28,39] except adding a closed 3D monitor box around the PS bead for the force calculations and placing two planar monitors above and below the membrane for recording the reflection and transmission spectra, respectively. The intensity of the incident field was defined as 1 unit. A nonuniform mesh grid size distribution was applied with a smallest mesh size of 1 nm around the PS bead and inside the nanopore. The trapping force on the 20 nm PS bead (shown in Figure 6) was calculated using the Maxwell stress tensor method.[40] While in calculations for the transmission and field enhancement spectra (shown in Figure 6), 18 nm PS bead was applied, leaving a gap between the bead and the edge of the nanopore for monitoring the field intensity. The selection of the bead size is in agreement with specification of the particles used in the experiment.

■ ASSOCIATED CONTENT

Ⓢ Supporting Information

Additional information on the position-dependent transmission intensity fluctuations and the discussion on the FoM. This material is available free of charge via the Internet at http://pubs.acs.org.

■ AUTHOR INFORMATION

Corresponding Author

*E-mail: pol.vandorpe@imec.be; romain.quidant@icfo.es.

Author Contributions

¶These authors contributed equally.

■ ACKNOWLEDGMENTS

This work was supported by the Spanish Ministry of Sciences through grants FIS2010 12834 and CSD2007-046-Nano-Light.es and Fundació Privada CELLEX Barcelona. C.C. gratefully acknowledges the SBA scholarship from Katholieke Universiteit Leuven, and P.V.D. gratefully acknowledges financial support from the FWO (Flanders). We also gratefully thank Prof. Reuven Gordon and Dr. Yuanjie Pang at University of Victoria for the useful discussions.

■ REFERENCES

(1) Nie, S. M.; Emory, S. R. *Science* **1997**, *275* (5303), 1102–1106.
(2) Willets, K. A.; Van Duyne, R. P. *Annu. Rev. Phys. Chem.* **2007**, *58*, 267–297.
(3) Jain, P. K.; El-Sayed, I. H.; El-Sayed, M. A. *Nano Today* **2007**, *2* (1), 18–29.
(4) Aslan, K.; Lakowicz, J. R.; Geddes, C. D. *Curr. Opin. Chem. Biol.* **2005**, *9* (5), 538–544.
(5) Luo, X. G.; Ishihara, T. *Opt. Express* **2004**, *12* (14), 3055–3065.
(6) Shao, D. B.; Chen, S. C. *Appl. Phys. Lett.* **2005**, *86* (25), 253107.
(7) Liu, Z. W.; Lee, H.; Xiong, Y.; Sun, C.; Zhang, X. *Science* **2007**, *315* (5819), 1686.
(8) De Angelis, F.; Das, G.; Candeloro, P.; Patrini, M.; Galli, M.; Bek, A.; Lazzarino, M.; Maksymov, I.; Liberale, C.; Andreani, L. C.; Di Fabrizio, E. *Nat. Nanotechnol.* **2010**, *5* (1), 67–72.
(9) Pillai, S.; Catchpole, , K. R.; Trupke, , T.; Green, , M. A. *J. Appl. Phys.* **2007**, *101* (9), 2734885.
(10) Atwater, H. A.; Polman, A. *Nat. Mater.* **2010**, *9* (3), 205–213.
(11) Barnes, W. L.; Dereux, A.; Ebbesen, T. W. *Nature* **2003**, *424* (6950), 824–830.
(12) Garcia-Vidal, F. J.; Martin-Moreno, L.; Ebbesen, T. W.; Kuipers, L. *Rev. Mod. Phys.* **2010**, *82* (1), 729–787.
(13) Neutens, P.; Van Dorpe, P.; De Vlaminck, I.; Lagae, L.; Borghs, G. *Nat. Photonics* **2009**, *3* (5), 283–286.
(14) Volpe, G.; Quidant, R.; Badenes, G.; Petrov, D. *Phys. Rev. Lett.* **2006**, *96* (23), 238101.
(15) Novotny, L.; Bian, R. X.; Xie, X. S. *Phys. Rev. Lett.* **1997**, *79* (4), 645–648.
(16) Xu, H. X.; Kall, M. *Phys. Rev. Lett.* **2002**, *89* (24), 246802.
(17) Grigorenko, A. N.; Roberts, N. W.; Dickinson, M. R.; Zhang, Y. *Nat. Photonics* **2008**, *2* (6), 365–370.
(18) Righini, M.; Zelenina, A. S.; Girard, C.; Quidant, R. *Nat. Phys.* **2007**, *3* (7), 477–480.
(19) Yang, A. H. J.; Moore, S. D.; Schmidt, B. S.; Klug, M.; Lipson, M.; Erickson, D. *Nature* **2009**, *457* (7225), 71–75.
(20) Juan, M. L.; Gordon, R.; Pang, Y. J.; Eftekhari, F.; Quidant, R. *Nat. Phys.* **2009**, *5* (12), 915–919.
(21) Miao, X. Y.; Lin, L. Y. *Opt. Lett.* **2007**, *32* (3), 295–297.
(22) Righini, M.; Ghenuche, P.; Cherukulappurath, S.; Myroshnychenko, V.; de Abajo, F. J. G.; Quidant, R. *Nano Lett.* **2009**, *9* (10), 3387–3391.
(23) Zhang, W. H.; Huang, L. N.; Santschi, C.; Martin, O. J. F. *Nano Lett.* **2010**, *10* (3), 1006–1011.

(24) Ashkin, A.; Dziedzic, J. M.; Bjorkholm, J. E.; Chu, S. *Opt. Lett.* **1986**, *11* (5), 288−290.
(25) Hajizadeh, F.; Reihani, S. N. S. *Opt. Express* **2010**, *18* (2), 551−559.
(26) Hansen, P. M.; Bhatia, V. K.; Harrit, N.; Oddershede, L. *Nano Lett.* **2005**, *5* (10), 1937−1942.
(27) Jauffred, L.; Oddershede, L. B. *Nano Lett.* **2010**, *10* (5), 1927−1930.
(28) Chen, C.; Lagae, L.; Maes, G.; Borghs, G.; Van Dorpe, P. *Phys. Stat. Sol. (RRL)* **2010**, *4* (10), 247−249.
(29) Acimovic, S. S.; Kreuzer, M. P.; Gonzalez, M. U.; Quidant, R. *ACS Nano* **2009**, *3* (5), 1231−1237.
(30) Pang, Y.; Gordon, R. *Nano Lett.* **2011**, *11* (9), 3763−3767.
(31) Dempster, A. P.; Laird, N. M.; Rubin, D. B. *J. R. Stat. Soc. B* **1977**, *39* (1), 1−38.
(32) Rabiner, L. R. *Proc. of IEEE* **1989**, *77* (2), 257−286.
(33) Piliarik, M.; Kvasnicka, P.; Galler, N.; Krenn, J. R.; Homola, J. *Opt. Express* **2011**, *19* (10), 9213−9220.
(34) Kwak, E. S.; Onuta, T. D.; Amarie, D.; Potyrailo, R.; Stein, B.; Jacobson, S. C.; Schaich, W. L.; Dragnea, B. *J. Phys. Chem. B* **2004**, *108* (36), 13607−13612.
(35) In order to define the FoM, the field enhancement factor is mandatory. In the case of near-field approaches, only the experimental realization provided with sufficient information has been considered.
(36) Harada, Y.; Asakura, T. *Opt. Commun.* **1996**, *124* (5−6), 529−541.
(37) Clarke, J.; Wu, H. C.; Jayasinghe, L.; Patel, A.; Reid, S.; Bayley, H. *Nat. Nanotechnol.* **2009**, *4* (4), 265−270.
(38) Chen, C.; Hutchison, J. A.; Van Dorpe, P.; Kox, R.; De Vlaminck, I.; Uji-i, H.; Hofkens, J.; Lagae, L.; Maes, G.; Borghs, G. *Small* **2009**, *5* (24), 2876−2882.
(39) Chen, C.; Verellen, N.; Lodewijks, K.; Lagae, L.; Maes, G.; Borghs, G.; Van Dorpe, P. *J. Appl. Phys.* **2010**, *108* (3), 034319.
(40) Rockstuhl, C.; Herzig, H. P. *J. Opt. A: Pure Appl. Opt.* **2004**, *6* (10), 921−931.

dx.doi.org/10.1021/nl2031458 | *Nano Lett.* 2012, 12, 125−132